



Synthesis and characterization of Pd(0), PdS, and Pd@PdO core-shell nanoparticles by solventless thermolysis of a Pd-thiolate cluster

Deepa Jose, Balaji R. Jagirdar*

Department of Inorganic and Physical Chemistry, Indian Institute of Science, Bangalore 560 012, India

ARTICLE INFO

Article history:

Received 16 April 2010

Received in revised form

13 June 2010

Accepted 12 July 2010

Available online 15 July 2010

Keywords:

Palladium nanoparticles

Thermolysis

Solvated metal atom dispersion

Core-shell

Colloid

ABSTRACT

Colloids of palladium nanoparticles have been prepared by the solvated metal atom dispersion (SMAD) method. The as-prepared Pd colloid consists of particles with an average diameter of 2.8 ± 0.1 nm. Digestive ripening of the as-prepared Pd colloid, a process involving refluxing the as-prepared colloid at or near the boiling point of the solvent in the presence of a passivating agent, dodecanethiol resulted in a previously reported Pd-thiolate cluster, $[\text{Pd}(\text{SC}_{12}\text{H}_{25})_2]_6$ but did not render the expected narrowing down of the particle size distribution. Solventless thermolysis of the Pd-thiolate complex resulted in various Pd systems such as Pd(0), PdS, and Pd@PdO core-shell nanoparticles thus demonstrating its versatility. These Pd nanostructures have been characterized using high-resolution electron microscopy and powder X-ray diffraction methods.

© 2010 Elsevier Inc. All rights reserved.

1. Introduction

Solventless thermolysis of precursor metal complexes has been found to be a useful synthetic route for metal nanoparticles, metal oxides, metal chalcogenides, etc., of various shapes such as rods, disks, wires, belts, and platelets. The precursor serves as the source of the metal, chalcogen, and the capping agent [1–9]. The products obtained by solventless thermolysis are monodisperse which is due primarily to minimal inter-particle collision [1]. Korgel and co-workers employed this methodology to prepare a variety of nanorods and nanowires of Bi_2S_3 [2], nanobelts of $\text{Pb}_3\text{O}_2\text{Cl}_2$ [3], nanorods, nanoplatelets, and nanodisks of Cu_2S [4], and nanorods and triangular nanoprisms of NiS [5]. Cha et al. [6] obtained Fe_3O_4 and Ag nanoparticles by the solventless thermolysis of an oleate complex in the absence of a surfactant under low pressure. Synthesis of uniform Cu_2S nanowires via decomposition of a Cu thiolate precursor has been reported by Wu and co-workers [7]. Trioctylphosphine oxide (TOPO) capped PdS nanoparticles have been synthesized by thermolysis of $[\text{Pd}(\text{S}_2\text{CNMe}(\text{Hex}))_2]$ (Hex = n-hexyl) [8]. Thermolysis of Pd(II) complexes with xanthate ligands also gave PdS nanoparticles [9].

Palladium nanophases such as Pd(0), PdO, and PdS have potential applications in catalysis, electronics, and hydrogen storage [10–24]. Palladium nanoparticles are effective catalysts for Suzuki reactions in both aqueous and non-aqueous solvents [10],

α -alkylation of ketones and ring-opening alkylation of cyclic 1,3-diketones with primary alcohols [11], semi-hydrogenation of phenylacetylene [12], hydrogenation of olefins [13] and unsaturated alcohols [14], hydrodechlorination of chloroorganic compounds [15], etc. They exhibit excellent hydrogen uptake properties too [16]. PdO nanoparticles in porous silica micropores were found to be very good catalysts for the aerobic oxidation of benzyl alcohol in water [17]. PdO/CeO₂ supported on γ Al₂O₃ was found to be a very good catalyst for the oxidation of methane [18]. Supported PdO catalysts bring about the transformation of CH₄ to C₂H₆, CO, CO₂, H₂, and H₂O [19]. Pd-PdO nanoparticles anchored uniformly on the inner surface of TiO₂ nanotubes were found to show excellent photocatalytic activity [20]. PdO/TiO₂ films show enhanced visible light absorption during light illumination [21]. PdO/zirconia nanophase materials show unusual reversible hydrogen storage properties [22]. PdS is a semiconductor material, with a band gap energy ~ 2 eV, having potential applications in lithographic films and plates, photographic films, catalytic photoelectrodes and solar cells [23]. Thin films of PdS were found to be very useful materials in photovoltaic cells due to their high absorption coefficient, band gap of 1.6 eV, n-type conductivity, and adequate donor density [24].

Motivated by the diversity of applications of various palladium nanophases, we attempted to explore the thermolytic behavior of a palladium thiolate cluster, $[\text{Pd}(\text{SC}_{12}\text{H}_{25})_2]_6$. Herein, we report the synthesis and characterization of a variety of Pd nanophase materials such as Pd(0), Pd@PdO core-shell, and PdS by the solventless thermolysis of $[\text{Pd}(\text{SC}_{12}\text{H}_{25})_2]_6$ by a judicious choice of conditions. The Pd-thiolate complex was obtained by the

* Corresponding author. Fax: +91 80 2360 1552.

E-mail address: jagirdar@ipc.iisc.ernet.in (B.R. Jagirdar).

disintegration of Pd nanoclusters by dodecanethiol from a Pd-4-*tert*-butyltoluene-dodecanethiol colloid under reflux conditions.

2. Experimental section

2.1. Materials

Palladium foil (0.3 mm thickness) (99.95%) was purchased from Arora-Matthey, Kolkata, India. Tungsten crucibles were obtained from R.D. Mathis Company, California. 2-Butanone (HPLC grade), dodecanethiol, and 4-*tert*-butyltoluene were purchased from Aldrich. 2-Butanone was dried over K_2CO_3 and degassed by several freeze-pump-thaw cycles. Dodecanethiol and 4-*tert*-butyltoluene were used after purging with Ar for 30 min before each experiment.

2.2. Instrumentation

UV-visible spectra were recorded using a Perkin-Elmer Lambda 35 UV/vis spectrometer. Solventless thermolysis experiments were carried out using a programmable Thermolyne furnace. The TEM bright field images, plasma filtered TEM images, electron diffraction patterns, HRTEM, EF-TEM, and EDX analysis were obtained using a TECNAI F30 transmission electron microscope with a spatial resolution of 2 Å operating at 300 kV. The TEM samples were prepared by placing a 1 μ L drop containing the powder redispersed in EtOH on a Formvar-coated copper grid. The powder X-ray diffraction measurements were carried out using a Philips powder X-ray diffractometer. The TGA measurements were carried out using a Netzsch TG209 F1 instrument. The 1H NMR and MALDI mass spectra were recorded using an Avance Bruker 400 MHz spectrometer and ULTRALEX-TOF/TOF Bruker Daltonics spectrometer, respectively.

2.3. Synthesis of Pd-butanone-4-*tert*-butyltoluene-dodecanethiol colloid

The Pd-butanone-4-*tert*-butyltoluene-dodecanethiol colloids were prepared by the solvated metal atom dispersion (SMAD) method. The SMAD setup is described in detail in Ref. [25]. In a typical experiment the crucible was loaded with about 200 mg of Pd foil. Dodecanethiol (~9 mL) and 4-*tert*-butyltoluene (~20 mL) were taken at the bottom of the reactor after purging with Ar for 30 min. The Pd to dodecanethiol ratio was about 1:20 mmol. The crucible was heated resistively in vacuo and the metal vapor was cocondensed with 2-butanone (~100 mL) on the walls of the reactor which was kept at liquid N_2 temperature. The Pd/butanone matrix was allowed to melt down under Ar atmosphere after the complete vaporization of the metal and stirred with dodecanethiol and 4-*tert*-butyltoluene to get the Pd-butanone-4-*tert*-butyltoluene-dodecanethiol colloid. This colloid was siphoned under Ar atmosphere into a Schlenk tube.

2.4. Synthesis of $[Pd(SC_{12}H_{25})_2]_6$

Butanone was removed from the as-prepared Pd colloid (~100 mL) in vacuo and then the colloid was refluxed under Ar atmosphere for 3 h. Ethanol (250 mL) was added to this Pd sample and the mixture was allowed to stand at room temperature overnight. Complete precipitation of the Pd-thiolate complex $[Pd(SC_{12}H_{25})_2]_6$ was effected during this time. The pure product was obtained from the precipitate as an air stable yellow colored powder by column chromatography using n-hexane as the eluent. The yield was about 90% (0.850 g). Single crystals of the thiolate

complex were obtained from a concentrated solution of the complex in toluene by allowing the solvent to evaporate very slowly.

2.5. Preparation of Pd(0), Pd@PdO core-shell, and PdS nanoparticles

The Pd-thiolate powder was heated in air at 298 °C in air for 3 h resulting in free-standing Pd(0) nanoparticles. Heating the thiolate complex in air at higher temperatures like 325, 425 °C for 3 h gave free-standing Pd@PdO core-shell nanoparticles. The PdS nanoparticles were prepared by the solventless thermolysis as well as by solvothermolysis. In the solventless method, the Pd-thiolate complex was sealed under Ar atmosphere in a glass tube and it was heated at 430 °C for 3 h. We also prepared PdS nanoparticles from the Pd-thiolate complex by the solution thermolysis wherein the thiolate complex was dissolved in a minimum amount of 4-*tert*-butyltoluene and the resulting solution was refluxed vigorously at 198 °C for 6 h under H_2 during which time, PdS nanoparticles precipitated out as a black powder.

3. Results and discussion

3.1. Behavior of the as-prepared Pd-butanone-4-*tert*-butyltoluene-dodecanethiol colloid under reflux conditions

Colloids of palladium nanoparticles were prepared by the solvated metal atom dispersion (SMAD) method [26]. The as-prepared Pd-butanone-4-*tert*-butyltoluene-thiol colloid was blackish brown in color consisting of spherical Pd nanoparticles [26]. Removal of butanone from the as-prepared colloid followed by refluxing under an atmosphere of Ar resulted in a yellow colored solution that showed absorption maxima at 415 and 313 nm with a shoulder at 369 nm (Fig. 1). The TEM bright field image of this sample did not show the presence of any nanoparticles (see Supplementary material). The unambiguous characterization of the product was established using NMR, MALDI mass, and FTIR spectroscopy, powder and single crystal X-ray crystallography as a tiara-shaped Pd-thiolate complex $[Pd(SC_{12}H_{25})_2]_6$ (see Supplementary material). The same

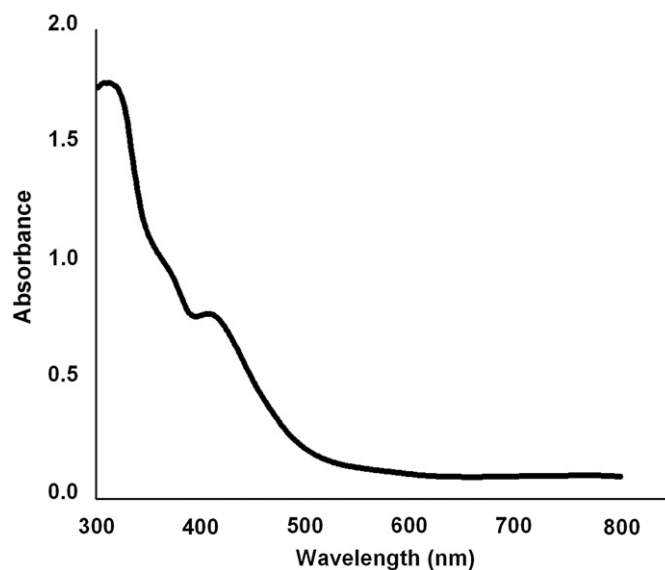


Fig. 1. UV-visible spectrum of Pd-4-*tert*-butyltoluene-dodecanethiol colloid after refluxing under Ar atmosphere for 3 h.

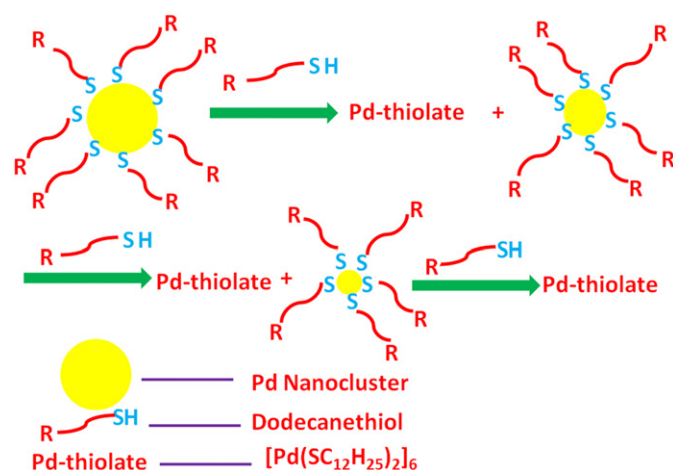
complex was previously synthesized by Klabunde and co-workers by a different route [27].

Refluxing the as-prepared polydisperse dodecanethiol capped SMAD-prepared Au, Ag, Cu, and Zn colloids gave highly monodisperse samples [28] via a process called as digestive ripening, wherein large clusters break down and the smaller clusters grow in size until a uniform size is reached for the entire colloid [29]. However, refluxing the dodecanethiol capped Pd colloids in 4-*tert*-butyltoluene did not result in a monodisperse sample, instead, a Pd–thiolate complex formed. The alkanethiolates protected Pd nanoparticles were found to undergo a dynamic growth process where initially larger particles are quickly formed followed by a decomposition into smaller clusters and finally to Pd ionic complexes [30]. Tsukuda et al. proposed a mechanism for the decomposition of thiolate protected Pd clusters in which the thiolate moieties detach from the Pd cores preferentially from the edge and vertex sites [31]. The free thiol ligand can further act as an etchant against the vertices and edges where the packing density is less due to self-dissociation.

Removal of butanone in effect replaces butanone, the initial capping agent with dodecanethiol as the final capping agent on Pd nanoparticles. Presence of excess thiol results in ligand exchange between the free thiol and the thiol bound to Pd nanoparticles. Schmid observed that the free and the bound surfactants undergo rapid exchange in the case of PPh₃ capped Au nanoparticles [32]. During the ligand exchange process, the bound thiol takes with it the surface atom or atoms from the Pd cluster due to the weak Pd–Pd interactions [33]. A redox reaction involving oxidation of Pd and reduction of the thiol resulted in the formation of the Pd–thiolate complex. Essentially, the thiol causes the leaching of Pd clusters to give the Pd–thiolate complex. An experiment in which the Pd:dodecanethiol ratio was 1:1 gave only a small amount of the Pd(II)–thiolate complex. This indicates that the presence of excess thiol is required for the complete leaching of Pd clusters. The transformation of the Pd nanoparticles to the Pd–thiolate complex is schematically shown in Scheme 1.

3.2. Solventless thermolysis of [Pd(SC₁₂H₂₅)₂]₆

We examined the thermal behavior of the [Pd(SC₁₂H₂₅)₂]₆ complex in the temperature range 30–1000 °C in air (Fig. 2) as well as under an Ar atmosphere (see Supplementary material). Initially, the loss of the hydrocarbon part (~68%) of the Pd–thiolate complex was noted at ~285 °C, followed by the loss



Scheme 1. Transformation of Pd nanoparticles into the Pd–thiolate complex [Pd(SC₁₂H₂₅)₂]₆.

of sulfur moiety in both air and under Ar at ~325 °C. Then a small increase in weight owing to the oxidation of Pd(0) to PdO was noted, when the TG analysis was carried out in air at ~400 °C. However, the percentage weight increase in air (~4.5%, inset Fig. 2) does not account for the complete conversion (the increase in wt% if complete oxidation takes place is ~15%) of Pd(0) to PdO suggesting that some Pd(0) still remains unoxidized even at high temperature. No oxidation of Pd(0) takes place when the thermal studies were carried out under Ar atmosphere. The grayish black powder obtained after TG analysis of [Pd(SC₁₂H₂₅)₂]₆ in air was confirmed as Pd(0) by powder XRD studies (see Supplementary material).

Taking clues from the TGA studies, we attempted to arrest the individual steps by thermolyzing the Pd–thiolate complex at different temperatures in the absence of any solvent. Thus, we were able to realize various Pd systems like Pd(0), PdS, and Pd@PdO core–shell nanoparticles. The details of solventless thermolysis and solvothermalolysis of the Pd–thiolate complex are summarized in Table 1.

3.3. Pd(0) nanoparticles

As is evident from the data in Table 1, the thiolate complex is stable up to 270 °C. Thermolysis of the compound at 270 °C left the powder XRD pattern unchanged from that of the thiolate complex (Fig. 3). Raising the thermolysis temperature to 298 °C resulted in the formation of bare Pd(0) nanoclusters. The color of the powder changed from yellow to black. The powder XRD

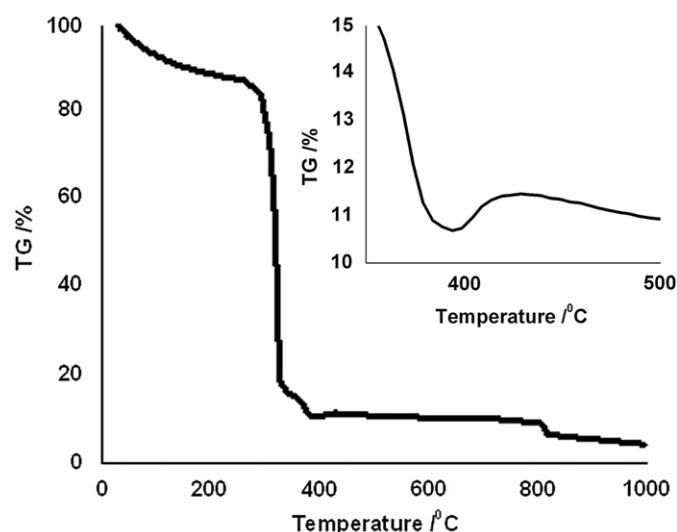


Fig. 2. TGA of [Pd(SC₁₂H₂₅)₂]₆ in air. Inset: weight increase during heating in air.

Table 1
Thermolysis of [Pd(SC₁₂H₂₅)₂]₆.

Temperature (°C)	Atmosphere	Product
200	Air	Pd–thiolate ^a
270	Air	Pd–thiolate
298	Air	Pd(0)
325	Air	Pd@PdO core–shell
425	Air	Pd@PdO core–shell
430	Argon	PdS
198 ^b	Hydrogen	PdS

^a Starting material unchanged at these temperatures.

^b Solvothermalolysis.

pattern shows that the sample is not fully crystalline having some amorphous material (Fig. 4a). Redispersion of the Pd(0) nanoparticles in ethanol followed by TEM studies (Fig. 4b) revealed the presence of elongated, oval-shaped particles of size ranging from 13 to 22 nm. The polydispersity of the particles is due to the absence of a surfactant, use of which would result in tuning the particle size. Ring-like diffraction patterns with spots

corresponding to the (111), (200), (220), (311), (222), (400), (331) and (420) planes of Pd(0) were noted in the SAED pattern (Fig. 4c). The EDX analysis (Fig. 4d) also confirmed the presence of Pd.

3.4. Pd@PdO core-shell nanoparticles

Solventless thermolysis of $[\text{Pd}(\text{SC}_{12}\text{H}_{25})_2]_6$ complex at 325 °C in air led to a Pd/PdO system as per the powder XRD studies (red trace, Fig. 5). The powder XRD pattern showed both FCC Pd

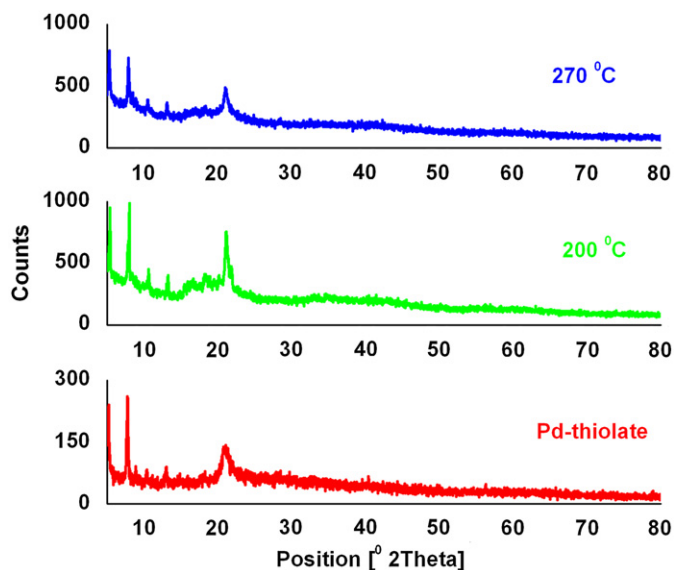


Fig. 3. Powder XRD pattern of $[\text{Pd}(\text{SC}_{12}\text{H}_{25})_2]_6$ before and after thermolysis at 200 and 270 °C in air.

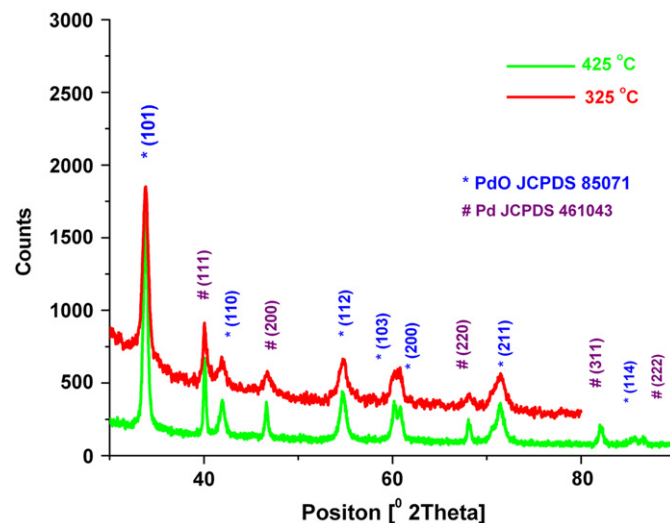


Fig. 5. Powder XRD pattern of Pd@PdO formed by the solventless thermolysis of $[\text{Pd}(\text{SC}_{12}\text{H}_{25})_2]_6$ at 325 and 425 °C in air.

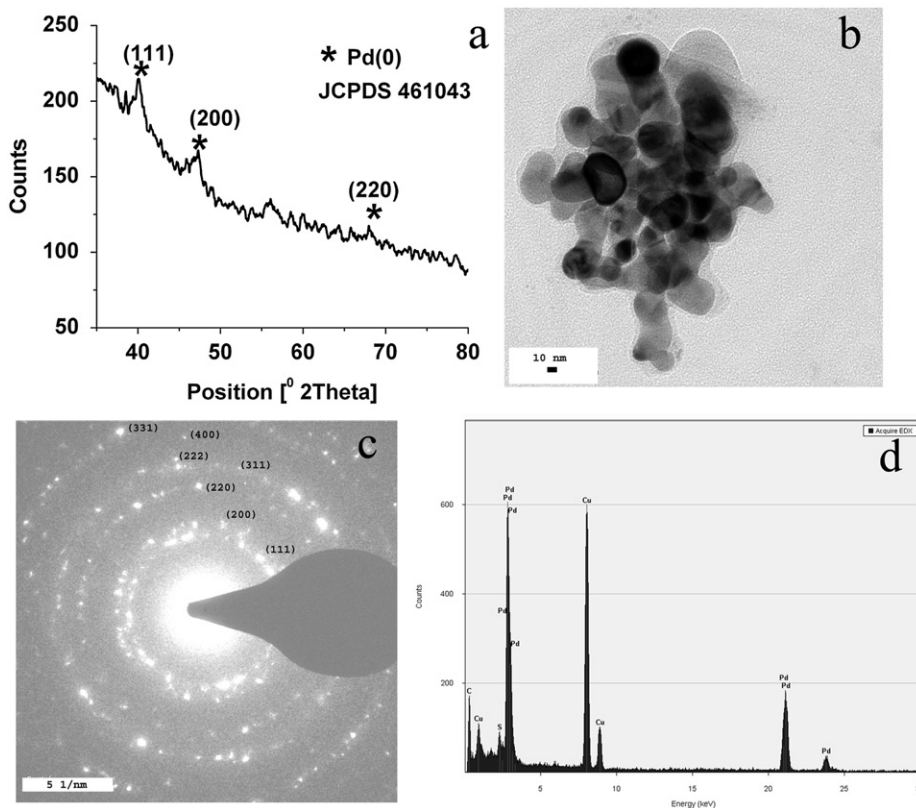


Fig. 4. (a) Powder XRD pattern, (b) TEM bright field image, (c) SAED pattern, and (d) EDX analysis of Pd(0) formed by the solventless thermolysis of $[\text{Pd}(\text{SC}_{12}\text{H}_{25})_2]_6$ at 298 °C in air.

and tetragonal PdO phases: reflections from the (111), (200) and (220) planes of Pd(0) and (101), (110), (112), (103) and (211) planes of PdO were observed (JCPDS file numbers 461043 and 850713). Complete oxidation of Pd to PdO did not take place even at higher temperatures (425 °C) suggesting a core–shell structure consisting of a shell of PdO protecting a Pd(0) core (green trace, Fig. 5). The average crystallite size calculated from the powder XRD pattern using the Scherrer formula was found to be about 54 nm.

The Pd@PdO core–shell structure was confirmed by detailed electron microscopy studies. The TEM bright field image (Fig. 6a) showed a broad distribution of polygonal shaped particles with size varying from 20 to 100 nm. The SAED pattern (Fig. 6b) confirmed the presence of both Pd and PdO phases. The HRTEM image (Fig. 6c) showed lattice fringes indicating the crystalline nature of the sample. The interplanar distance calculated from the HRTEM image gave two different d values: 2.25 Å of the (111) plane of Pd in the core and 2.63 Å of the (101) plane of PdO in the shell region. Further, the existence of both Pd and PdO phases in the same cluster was confirmed by EDX analysis. The EDX analysis of an isolated cluster showed the presence of both Pd and O in 96 and 4 wt%, respectively (see Supplementary Material). In addition, the energy-filtered TEM (EFTEM) images (Fig. 6d and e) showed

the presence of both Pd and O in the same cluster. Oxygen was found to be concentrated on the surface of the cluster. The bright contrast in Fig. 6d corresponds to Pd and the bright contrast in Fig. 6e corresponds to O. Thus the combined powder XRD and electron microscopy results revealed the formation of a core–shell structure of Pd@PdO.

Once Pd(0) formed, dissociative adsorption of oxygen takes place on the surface of the particles. This is followed by the diffusion of oxygen atoms into the Pd lattice by forcing apart the Pd atoms to give PdO at 425 °C. The surface oxidation of Pd to PdO has been studied by others [34]. Complete oxidation of Pd(0) to PdO was not observed in our case and this could be due to the diffusion of oxygen only onto the surface layers. The PdO layer was found to be quite stable, heating the core–shell structure at higher temperatures did not result in the oxidation of the core which suggested that PdO formed a good protective shell over the Pd core [35].

3.5. PdS nanoparticles

Solventless thermolysis of the Pd–thiolate complex at 430 °C under Ar resulted in PdS nanopowder. The powder X-ray

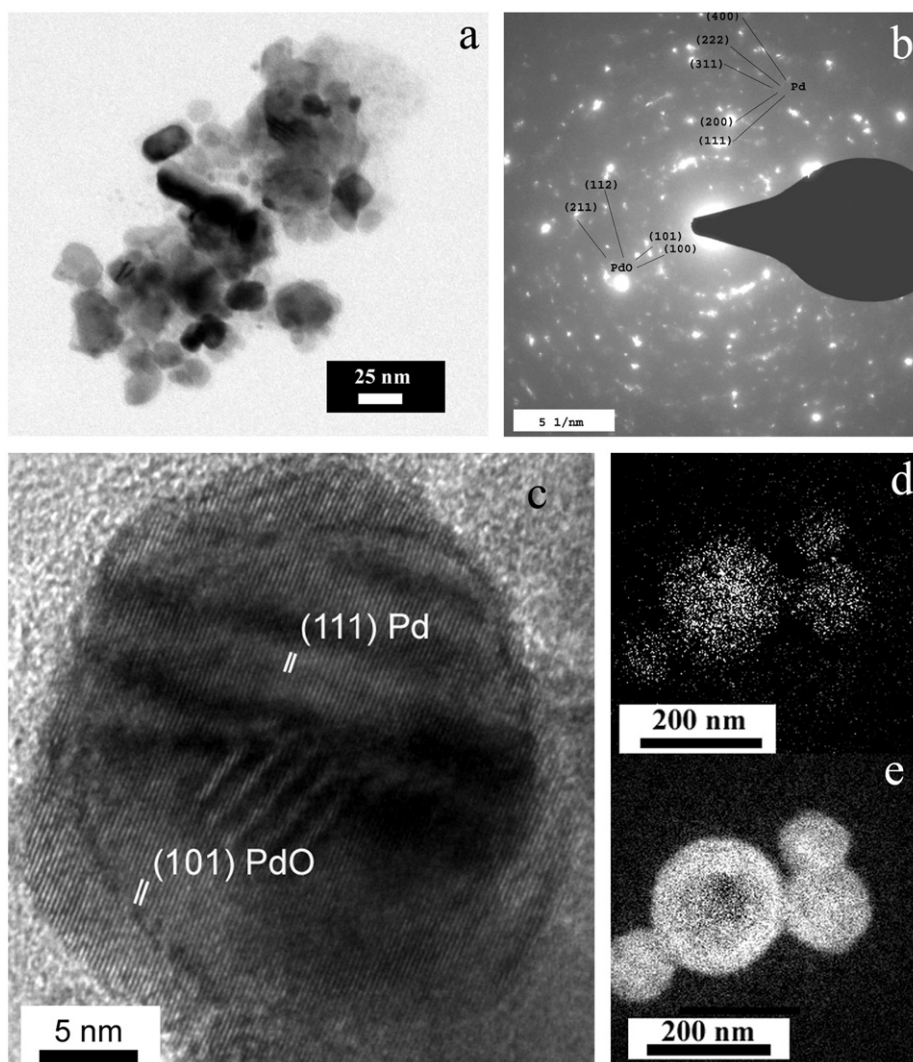


Fig. 6. (a) TEM bright field image, (b) SAED pattern, (c) HRTEM image, (d) EFTEM Pd mapping, and (e) EFTEM O mapping of Pd@PdO formed by the solventless thermolysis of $[\text{Pd}(\text{SC}_{12}\text{H}_{25})_2]_6$ at 425 °C in air.

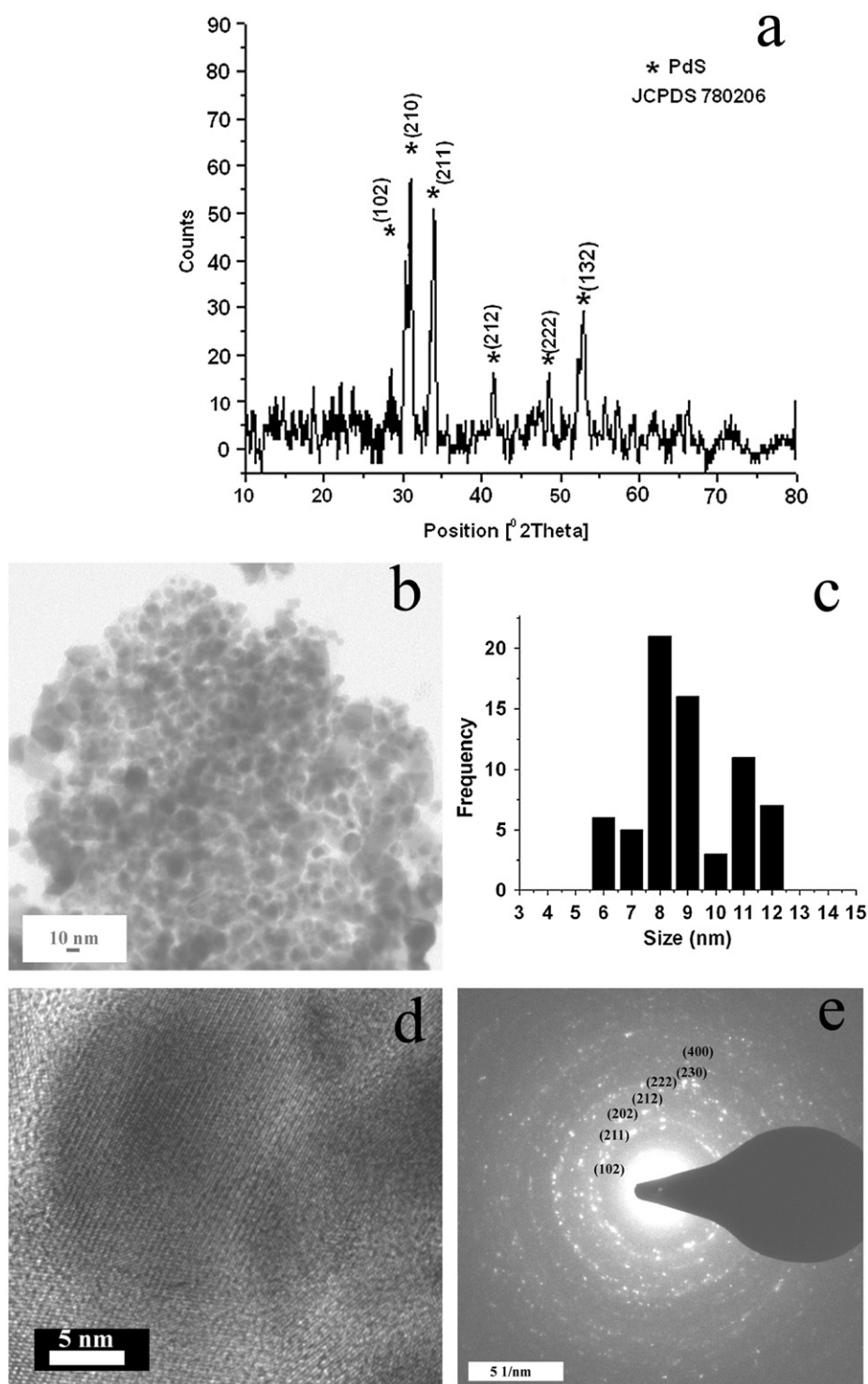


Fig. 7. (a) Powder XRD pattern, (b) TEM bright field image, (c) histogram showing particle size distribution, (d) HRTEM image, and (e) SAED pattern of PdS formed by the solventless thermolysis of $[\text{Pd}(\text{SC}_{12}\text{H}_{25})_2]_6$ at 430 °C under Ar.

diffraction pattern (Fig. 7a) of the black powder showed reflections corresponding to the tetragonal phase of PdS and could be indexed to the (102), (210), (211), (212), (222) and (132) planes (JCPDS#780206). The TEM bright field image (Fig. 7b) revealed the presence of spherical PdS nanoclusters with a size of 9.2 ± 0.9 nm (Fig. 7c). The sample was found to be highly crystalline as evidenced by the presence of clear lattice fringes in the HRTEM image (Fig. 7d). In addition, the SAED pattern (Fig. 7e) could be indexed to that of PdS. The EDX analysis

of several isolated clusters gave an average composition of 77% Pd and 23% S (see Supplementary Material).

3.6. Solvothermal hydrogenolysis of Pd–thiolate complex

Solvothermal synthesis of Pd–dodecanethiolate complex at 259 °C in diphenyl ether under Ar atmosphere gave PdS nanoparticles [27]. In our hands, solvothermal synthesis carried out in *tert*-butyltoluene

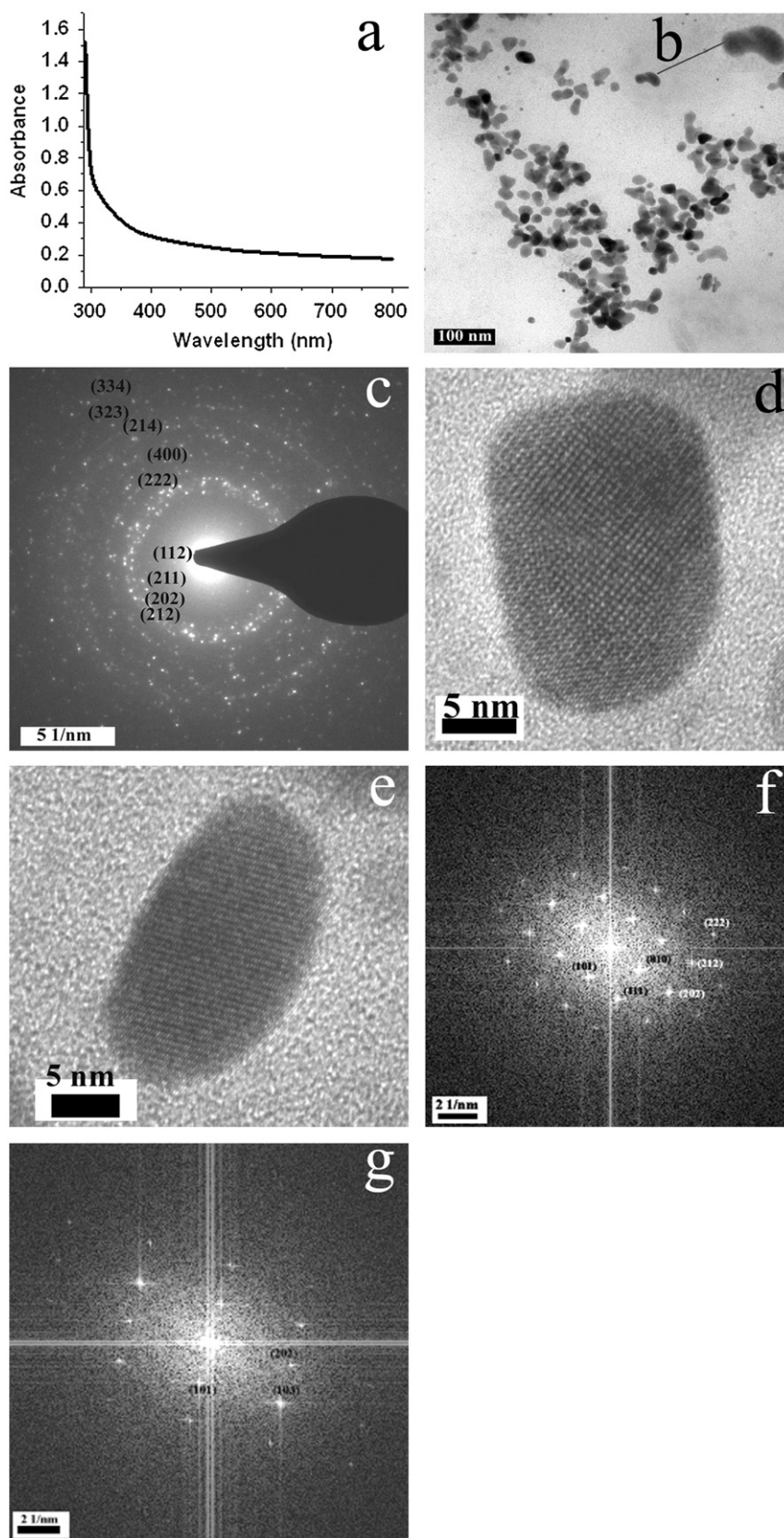
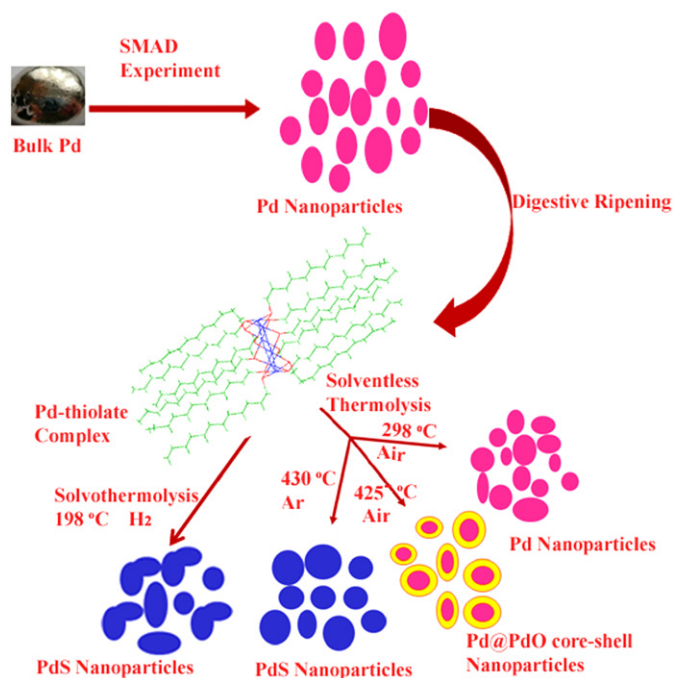


Fig. 8. (a) UV-visible spectrum, (b) TEM bright field image, (c) SAED pattern, (d) HRTEM image showing crystal growth along the $\langle 101 \rangle$ direction, (e) HRTEM image showing crystal growth along the $\langle 010 \rangle$ direction, (f) FFT pattern corresponding to the HRTEM image in (d), and (g) FFT pattern corresponding to the HRTEM image in (e) of PdS formed by the solvothermal synthesis of $[\text{Pd}(\text{SC}_{12}\text{H}_{25})_2]_6$ at 198 °C under H_2 .



Scheme 2. Formation of various Pd nanophases from Pd nanoparticles.

under reflux conditions (198 °C) under H₂ atmosphere resulted in the yellow colored solution turning colorless accompanied by the formation of a black precipitate of PdS. The UV–visible spectrum (Fig. 8a) of the sample after 6 h of reflux became featureless. The TEM bright field image (Fig. 8b) showed well separated spherical nanoparticles of average diameter 13 nm. In addition to the spherical particles, some elongated necked particles formed by the coalescence of two spherical particles were also noted. The SAED pattern (Fig. 8c) could be indexed to the (112), (211), (202), (212), (222), (400), (214), (323) and (334) planes of tetragonal PdS (JCPDS#780206). The HRTEM images (Fig. 8d and e) of some of the elongated particles show crystal growth along the $\langle 101 \rangle$ and $\langle 010 \rangle$ directions, respectively. The corresponding FFT patterns are shown in (Fig. 8f and g).

The entire sequence of events described above has been summarized pictorially in Scheme 2. As shown in the scheme, palladium nanoparticles have been obtained from bulk palladium by a top down approach, solvated metal atom dispersion. Refluxing of this as-prepared Pd colloid gave a Pd–thiolate cluster, [Pd(SC₁₂H₂₅)₂]₆. When the palladium thiolate complex was subjected to solventless thermolysis, various Pd nanophase materials were obtained depending upon the reaction conditions.

4. Conclusions

In conclusion, we have prepared colloids of Pd nanoparticles stabilized by dodecanethiol ligand by the solvated metal atom dispersion (SMAD) method. The as-prepared colloid consisting of Pd nanoparticles of average diameter 2.8 ± 0.1 nm was transformed into a palladium thiolate cluster, [Pd(SC₁₂H₂₅)₂]₆ upon refluxing, instead of the expected narrowing down of the size distribution via a process called as digestive ripening. The Pd–thiolate complex is a very versatile precursor for the synthesis of various Pd nanophase materials such as Pd(O), PdS, and Pd@PdO core–shell systems devoid of any capping agents

via solventless thermolysis methods. Such versatility is unprecedented.

Acknowledgments

We are grateful to the Council of Scientific and Industrial Research, India, for financial support. We thank the I.I.Sc. Institute Nanoscience Initiative and the Solid State and Structural Chemistry Unit, I.I.Sc. for allowing us to access the microscopic facilities and the powder X-ray diffractometer, respectively. D.J. thanks the CSIR for a fellowship.

Appendix A. Supporting materials

Supplementary data associated with this article can be found in the online version at doi:10.1016/j.jssc.2010.07.013.

References

- [1] T. Teranishi, S. Hasegawa, T. Shimizu, M. Miyake, *Adv. Mater.* 13 (2001) 1699–1701.
- [2] M.B. Sigman, B.A. Korgel, *Chem. Mater.* 17 (2005) 1655–1660.
- [3] M.B. Sigman, B.A. Korgel, *J. Am. Chem. Soc.* 127 (2005) 10089–10095.
- [4] (a) T.H. Larsen, M. Sigman, A. Ghezelbash, R.C. Doty, B.A. Korgel, *J. Am. Chem. Soc.* 125 (2003) 5638–5639; (b) M.B. Sigman, A. Ghezelbash, T. Hanrath, A.E. Saunders, F. Lee, B.A. Korgel, *J. Am. Chem. Soc.* 125 (2003) 16050–16057.
- [5] A. Ghezelbash, M.B. Sigman, B.A. Korgel, *Nano Lett.* 4 (2004) 537–542.
- [6] H.G. Cha, D.K. Lee, Y.H. Kim, C.W. Kim, C.S. Lee, Y.S. Kang, *Inorg. Chem.* 47 (2008) 121–127.
- [7] L. Chen, Y. -B. Chen, L. -M. Wu, *J. Am. Chem. Soc.* 126 (2004) 16334–16335.
- [8] M.A. Malik, P. O'Brien, N. Revaprasadu, *J. Mater. Chem.* 12 (2002) 92–97.
- [9] A. Singhal, D.P. Dutta, A.K. Tyagi, S.M. Mobin, P. Mathur, I. Lieberwirth, *J. Organomet. Chem.* 692 (2007) 5285–5294.
- [10] G. Wei, W. Zhang, F. Wen, Y. Wang, M. Zhang, *J. Phys. Chem. C* 112 (2008) 10827–10832.
- [11] Y.M.A. Yamada, Y. Uozumi, *Tetrahedron* 63 (2007) 8492–8498.
- [12] S. Dominguez-Dominguez, A. Berenguer-Murcia, B.K. Pradhan, Á. Linares-Solano, D. Cazorla-Amorós, *J. Phys. Chem. C* 112 (2008) 3827–3834.
- [13] C. -B. Hwang, Y. -S. Fu, Y. -L. Lu, S. -W. Jang, P. -T. Chou, C.R.C. Wang, S.J. Yu, *J. Catal.* 195 (2000) 336–341.
- [14] S. Kidambi, J. Dai, J. Li, M.L. Bruening, *J. Am. Chem. Soc.* 126 (2004) 2658–2659.
- [15] D. Fritsch, K. Kuhr, K. Mackenzie, F. -D. Kopinke, *Catal. Today* 82 (2003) 105–118.
- [16] (a) H. Kobayashi, M. Yamauchi, H. Kitagawa, Y. Kubota, K. Kato, M. Takata, *J. Am. Chem. Soc.* 130 (2008) 1828–1829; (b) M. Yamauchi, H. Kitagawa, *Synth. Mater.* 153 (2005) 353–356; (c) D.S. Sibirtsev, A.V. Skripov, N. Natter, R. Hemptmann, *Solid State Commun.* 108 (1998) 583–586.
- [17] K. Wada, K. Yano, T. Kondo, T. -A. Mitsudo, *Catal. Today* 117 (2006) 242–247.
- [18] E. Kanazaki, S. Tanaka, K. -I. Murai, T. Moriga, J. Motonaka, M. Katoh, I. Nakabayashi, *Anal. Sci.* 20 (2004) 1069–1073.
- [19] K.R. Thampi, J. Kiwi, M. Grätzel, *Catal. Lett.* 4 (1990) 49–56.
- [20] H. Su, Q. Dong, J. Han, D. Zhang, Q. Guo, *Biomacromolecules* 9 (2008) 499–504.
- [21] Q. Li, W. Liang, J.K. Shang, *Appl. Phys. Lett.* 90 (2007) 063109/1–063109/3.
- [22] L.F. Chen, J.A. Wang, M.A. Valenzuela, X. Bokhimi, D.R. Acosta, O. Novaro, *J. Alloys Compd.* 417 (2006) 220–223.
- [23] J.C.W. Folmer, J.A. Turner, B.A. Parkinson, *J. Solid State Chem.* 68 (1987) 28–37.
- [24] I.J. Ferrer, P. Díaz-Chao, A. Pascual, C. Sánchez, *Thin Solid Films* 515 (2007) 5783–5786.
- [25] K.J. Klabunde, P.L. Timms, P.S. Skell, S. Ittel, *Inorg. Synth.* 19 (1979) 59–86.
- [26] D. Jose, B.R. Jagirdar, *J. Phys. Chem. C* 112 (2008) 10089–10094.
- [27] Z. Yang, A.B. Smetana, C.M. Sorensen, K.J. Klabunde, *Inorg. Chem.* 46 (2007) 2427–2431.
- [28] (a) A.B. Smetana, K.J. Klabunde, C.M. Sorensen, *J. Colloid Interface Sci.* 284 (2005) 521–526; (b) S. Stoeva, K.J. Klabunde, C. Sorensen, I. Dragieva, *J. Am. Chem. Soc.* 124 (2002) 2305–2311; (c) S.B. Kalidindi, B.R. Jagirdar, *J. Phys. Chem. C* 112 (2008) 4042–4048.
- [29] X.M. Lin, C.M. Sorensen, K.J. Klabunde, *J. Nanopart. Res.* 2 (2000) 157–164.

- [30] S. Chen, K. Huang, J.A. Stearns, *Chem. Mater.* 12 (2000) 540–547.
- [31] H. Murayama, T. Narushima, Y. Negishi, T. Tsukuda, *J. Phys. Chem. B* 108 (2004) 3496–3503.
- [32] G. Schmid, *Struct. Bond.* 62 (1985) 51–85.
- [33] D.R. Lide, *CRC Handbook of Chemistry and Physics*, 80th ed., CRC Press, Boca Raton, 1999–2000.
- [34] (a) D. Zemlyanov, B. Aszalos-Kiss, E. Kleimenov, D. Teschner, S. Zafeiratos, M. Hävecker, A. Knop-Gericke, R. Schlögl, H. Gabasch, W. Unterberger, K. Hayek, B. Klötzer, *Surf. Sci.* 600 (2006) 983–994;
- (b) Y. Xiong, J. Chen, B. Wiley, Y. Xia, Y. Yin, Z.-Y. Li, *Nano Lett.* 5 (2005) 1237–1242;
- (c) G. Ketteler, D.F. Ogletree, H. Bluhm, H. Liu, E.L.D. Hebenstreit, M. Salmeron, *J. Am. Chem. Soc.* 127 (2005) 18269–18273;
- (d) E.H. Voogt, A.J.M. Mens, O.L.J. Gijzeman, J.W. Geus, *Surf. Sci.* 373 (1997) 210–220.
- [35] E. Lundgren, J. Gustafson, A. Mikkelsen, J.N. Andersen, A. Stierle, H. Dosch, M. Todorova, J. Rogal, K. Reuter, M. Scheffler, *Phys. Rev. Lett.* 92 (2004) 046101/1–046101/4.